Partial Discharge Activity in Rotating Machine Type II Insulation Systems as a Function of Temperature and Frequency

Torstein Grav Aakre, Emre Kantar, and Espen Eberg

***Abstract*—The main purpose of this study was to investigate if the application of very low frequencies for PD measurements in type II generator bar insulation is relevant when compared to applying power line frequency at different test temperatures. Laboratory experiments were performed on stator bars rated 6.4 kV and 7.4 kV, manufactured with both resin-rich (RR) and vacuum pressure impregnation (VPI) processes, and taken from service and back-up (pristine). The samples were preconditioned at the maximum test voltage of 1.5 U_0 before a frequency sweep was performed between 0.1 Hz and 50 Hz. The test temperature was varied between 20 °C and 155 °C. Investigation of cross sections of the generator bars was done to qualitatively describe the voids. The main results showed that the partial discharge inception voltage (PDIV) for RR was temperature independent at 50 Hz and decreased by 40 % at 0.1 Hz with increased temperatures, whereas the PDIV for VPI was frequency independent and increased by 70 % with temperature. Similarly, the PD magnitude and total apparent charge decreased by 90 % for VPI with increased temperature, whereas it more than doubled for RR with temperature. Bars manufactured with the RR process showed significantly larger voids, located close to the copper conductors, compared to VPI-manufactured bars, where voids were mainly located within the mainwall insulation. Results indicated that tests performed at 0.1 Hz cannot directly represent results obtained at 50 Hz. The use of a wide range of frequencies and test temperatures broaden the understanding of the behavior of the voids inside the mainwall insulation.**

***Index Terms*— Hydropower generator bar insulation, electrification, VLF, partial discharges, internal discharge.**

I. INTRODUCTION

OFF-LINE condition assessment of high-voltage equipment with a large capacitance, for example, generators and cables, is advantageous to perform at very low frequency (VLF) due to the small capacitive charging current compared to the power line frequency (PLF) sources that require considerably more resources to be operated. Relevant IEC and IEEE standards for condition assessment of hydropower stator insulation [1], [2] have been developed for power frequency testing but can be used for VLF and 400 Hz as well. The VLF is referred to as a possible condition assessment method in [3], but with the caution that VLF might produce different results than power line frequency. The electric field distribution along the end corona protection (ECP) on generator stator bars is, for example, frequency-dependent [4]. This extends the region with high voltage potential throughout the ECP section with 0.1 Hz compared to 50/60 Hz, which the ECP is designed for. Additionally, condition assessment is performed on hot or cold generators, depending on the waiting time between turning off the generator and when the measurements start, causing further complications if the test conditions vary.

There are two dominating production processes for type II generator bar insulation [5]: In the resin-rich (RR) process, prewetted insulation tapes are heated and cured under press, whereas in the vacuum pressure impregnation (VPI) process, dry tapes are wrapped around the copper conductor before the bar is impregnated under vacuum in order to remove voids. Experience has shown VPI insulation can be in good condition after more than 50 years of service [6]–[8]. The main defects inside the mainwall insulation are thus voids or delaminations depending on the success of the taping technique, curing, and deterioration during service [9]; RR is, for example, more prone to delaminations.

There exist just a few papers dealing with testing partial discharges (PD) in voids at different voltage frequencies and test temperatures. Model studies of defined, single voids in pure polymer materials are therefore included to show expected trends and possible mechanisms. Nair et al. [10] studied slot discharges between 0.1 Hz and 50 Hz between 20 °C and 60 °C, that is, 'voids' between the mainwall insulation and stator core. They observed that the total apparent charge per period (discharge current) and maximum apparent charge strongly increased with temperature and became frequency dependent as the temperature raised, with the highest values at 50 Hz. Further, in [11], only a variation in voltage frequency demonstrated an opposite frequency trend: The total apparent charge from internal delamination discharges was about 50 % higher at 0.1 Hz than at 50 Hz. The maximum apparent

Manuscript submitted XX XX. This work is funded by the project 'Hydrogenerator Stator Winding Insulation Assessment'. The project is supported by The Research Council of Norway (Project No. 255099/E20), and industrial partners. *(Corresponding author: T. Aakre).*

Torstein Grav Aakre was with the Department of Electric Power Engineering, Norwegian University of Technology and Science (NTNU), NO-7465 Trondheim, Norway. He is now with the Department of Electric Power Technology, SINTEF Energy Research, NO-7491 Trondheim, Norway (torstein.aakre@sintef.no).

Emre Kantar is with the Department of Electric Power Technology, SINTEF Energy Research, NO-7491 Trondheim, Norway (emre.kantar@sintef.no).

Espen Eberg is with the Department of Electric Power Technology, SINTEF Energy Research, NO-7491 Trondheim, Norway (espen.eberg@sintef.no).

Color versions of one or more of the figures in this article are available online at http://ieeexplore.ieee.org

charge was, however, only 60 – 70% at 0.1 Hz of what was measured at 50 Hz. A large cylindrical void in RR mainwall insulation was used as a model in [12] to mimic delaminations. It was found that the PD inception voltage was frequency independent below 90 °C. Above that, the Partial Discharge Inception Voltage (PDIV) at 0.1 Hz decreased and at 50 Hz remained unchanged. Similarly, in a polycarbonate sample [13], the measured number of PDs per cycle were frequency independent at PDIV, whereas increasing with frequency at higher voltages. Conversely, the average PD magnitude was frequency dependent at PDIV (increasing with frequency) but frequency independent at higher voltages. They explained the frequency dependence by a statistical time lag and the charge transport in the cavity surface at different applied frequencies [14]. Differences were seen for spherical voids in epoxy, as the maximum apparent charge was either decreasing with frequency in a 1 mm void in [15] or frequency independent in a 1.5 mm void in [16]. A possible mechanism was concluded to be a surface charge decay that might significantly influence PD behavior. The presented model studies show variations in PD behavior that need to be investigated for real stator bars.

The main purpose of this work is to compare partial discharges obtained at VLF (0.1 Hz) to those obtained at PLF (50 Hz) to evaluate if VLF is feasible for the condition assessment of type II machine insulation. The testing temperature is also introduced as a variable because off-line assessment often is performed at lower temperatures than the operating temperature of the machine. The work is conducted for both RR and VPI insulation systems.

II. Theoretical Background

It is often useful to compare results from unknown voids to simplified models, as this can provide insight into involved parameters and important trends. The theoretical background is therefore based on the very simplified case of a cylindrical void with a homogeneous gap giving rise to the abc-model. The void is in the theoretical treatment assumed to completely discharge in each discharge.

It is reasonable to assume Laplacian conditions before the first PD occurs; thus, the generalized abc-model can be assumed valid. The inception voltage U_s in homogeneous void gaps with void gap distance d_c is described experimentally by the Paschen curve [17]:

$$U_\mathrm{s} = 6.72\sqrt{pd_\mathrm{c}} + 24.36(pd_\mathrm{c}) + \frac{0.00411}{\sqrt{pd_\mathrm{c}}}\,[\mathrm{kV}]. \tag{1}$$

The expression is valid for pressure multiplied by distance, pd_c, values in the range of 10^{-3} to 10^{2} (bar·cm). An idealized void can be modeled as a capacitance and resistance in series with an insulation capacitance C, resistance R, and generic complex impedance $Z(\omega)$ measured by dielectric response, as illustrated in Fig. 1. This is an expansion of the capacitive abc-model [12].

Using this model, the initiation voltage U_i applied to the complete system to get PD inception U_s is

$$U_\mathrm{i} = \left(1 + \frac{d_\mathrm{b}}{d_\mathrm{c}} \frac{\sigma_\mathrm{c} + j\omega\varepsilon_0\varepsilon_{\mathrm{r,c}}}{\sigma_\mathrm{b} - \omega\mathrm{Im}\{\varepsilon_\mathrm{b}^*\} + j\omega\mathrm{Re}\{\varepsilon_\mathrm{b}^*\}}\right) \cdot U_\mathrm{s}, \tag{2}$$

where d_b is the insulation system thickness, d_c the void gap distance, σ_c and σ_b the conductivity of the void and insulation, respectively, ε_b^* the complex permittivity in the insulation, $\varepsilon_{\mathrm{r,c}}$ the relative permittivity of air, and ω the angular frequency. The conductivity is, in general, increasing with temperature according to the Arrhenius law

$$\sigma(T) = \sigma_0 \cdot e^{-\frac{E_\mathrm{a}}{k_\mathrm{B}T}}, \tag{3}$$

where k_B is Boltzmann's constant, σ_0 is a constant, and E_a is the activation energy, and T the temperature in Kelvin.

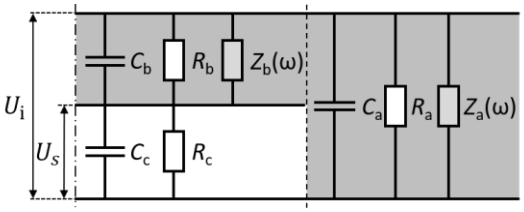

Fig. 1: Equivalent circuit of an insulation system with a void. The insulation is shaded grey, whereas the void is white.

The measured apparent charge within the simplified scheme can be approximated to

$$q_\mathrm{a} \approx C_\mathrm{b} \cdot (U_\mathrm{s} - U_\mathrm{r}), \tag{4}$$

where C_b is the capacitance in series with the void, U_s is the ignition voltage in the void and U_r is the remanent voltage. Similarly, the theoretical PD repetition rate per period is [14]

$$n = 4 \cdot \frac{U_0 - U_\mathrm{r}}{U_\mathrm{s} - U_\mathrm{r}}, \tag{5}$$

where U_0 is the maximum applied voltage across the void during a voltage cycle assuming no PDs and no remanent charges. The total apparent charge per period can be written as the product of repetition rate and apparent charge:

$$q_\mathrm{a}^\mathrm{T} = \sum q_\mathrm{a} = n_0 \cdot q_\mathrm{a} = 4 \cdot C_\mathrm{b} \cdot (U_0 - U_\mathrm{r}). \tag{6}$$

If then, assuming that many voids coexist within the same insulation system with approximately the same voltage, it is possible to sum all PDs in all voids by the superposition principle:

$$Q_\mathrm{a}^\mathrm{T} = \sum\nolimits_{\mathrm{voids}} q_\mathrm{a}^\mathrm{T} = 4 \cdot C_\mathrm{b}^\mathrm{TOT} \cdot (U_0 - U_\mathrm{r}). \tag{7}$$

where $C_\mathrm{b}^\mathrm{TOT}$ now represents the total series capacitance of all the voids. This means that the total apparent charge is expected to be linear with voltage.

Another approach to describe the PDs is to consider the available energy, $\mathcal{E}$, inside the void that can give rise to PDs is stored in the electric field by

$$\mathcal{E} = \frac{1}{2}\int \varepsilon_0\varepsilon_r\,|E|^2\,dV. \tag{8}$$

where V is the volume of the void. The energy is expressed as $\mathcal{E} = \frac{1}{2}U_0^2C_\mathrm{c} = \frac{1}{2}QU_0$ when the capacitance can be defined. Thus, the smaller the volume or electric field, the smaller the available energy, which implies that the available energy for PDs is reduced.

III. Materials and Methodology

A. Test Objects

Generator bars with two different type II insulation systems were tested, i.e., RR and VPI insulation with characteristic properties given in Table 1. The RR bars were cut to 50 cm in length to reduce the capacitance. Later, the VPI bars were tested with improved equipment enabling a longer sample of about 2 m. All test objects had the end windings removed, and a new ECP was applied according to the manufacturer's instructions. The bars were clamped between aluminum bars to ensure a defined ground potential and simulate a real stator slot.

TABLE 1
IMPORTANT SPECIFICATIONS OF THE TEST OBJECTS.

	RR	VPI
Total sample length (m)	0.5	2
Active length (m)	0.2	1.4
Strands (#)	18 parallel	64 Roebel
Cross section (mm x mm)	20x56	22x70
Insulation thickness (mm)	3	3.7
Rated voltage (U_0 kV_{rms})	6.4	7.4
Installation year	1976	1965
Years in service	35	52
Insulation type	MicaMat [18]	Micadur [19]
Binder	Polyester	Epoxy
Barrier	Mica	Mica
Backing	Glass-fiber cloth	Glass-fiber cloth

The bars were divided into two groups, as shown in Table 2. The VPI back-up bars were still back-up for a generator in service, and testing could not be destructive or degrade the bars by any chance. Hence, the maximum testing voltage and temperature were lower in these specific bars. An earlier published work for the screening of the VPI bars has shown no correlation between location and PD level [20]. The same was also observed for the RR bars, and the locations in the stator were not investigated.

TABLE 2
THE DIFFERENT TEST GROUPS

Service aged state	RR	VPI
Back-up bar (# samples)	3	2
HV terminal (# samples)	3	5
N terminal (# samples)	3	1

B. Material characteristics

A selected population of bars was characterized by dielectric spectroscopy at both a broad frequency and temperature range. The test objects were guarded mechanically with a 2-mm wide removal of the semiconducting paint to remove the effect of the ECP. The voltage frequency range was between 10^{-4} Hz to 10^{3} Hz, the applied voltage was 200 V, and the temperature was in the range of 20 °C to 155 °C.

Similarly, a polarization and depolarization test was performed on a selected population of the bars to find the DC conductivity, using a high-resolution setup for the RR bars [21] and a Megger MIT 252 for the VPI bars, which provide accurate results for type II insulation systems.

A selection of RR bars and VPI bars were cut into 1.5 cm thick sections after completing the electrical tests. The sections were polished and investigated for voids and delaminations in an optical microscope.

C. PD Test Setup

A sketch of the experimental test circuit for PD detection is shown in Fig. 2. The test object (stator bar) is situated in a heating cabinet. The measurement circuit is in compliance with IEC 60034-27 and calibrated according to IEC 60270. The measurement impedance is commercially available from Omicron, CPL 542, and is connected to the data processing unit MPD 600. The high-voltage signal is set by a DAQ or function generator and amplified by a TREK high-voltage amplifier in series with an RC low-pass filter, with a cut-off frequency of 1.5 kHz. Values for the involved capacitances and power sources are shown in Table 3.

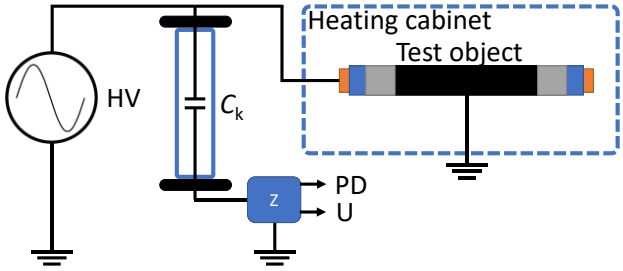

Fig. 2: Schematic of the PD test setup. It is based on a direct measurement where the PD signal is measured across an impedance Z in series with the measure capacitance C_k.

TABLE 3
TEST CIRCUIT ELEMENTS.

Test parameter	RR	VPI
Test object capacitance	400 pF	2.7 nF
Coupling capacitor	3.4 nF	2 nF
Power source	TREK 20/20B	TREK 30/30C

D. PD test procedure

The PD test procedure is given below with details for the given voltage frequencies, maximum voltage, number of voltage steps, preconditioning length, temperature range, and waiting time before a new PD test after a new temperature in Table 4:

1. Obtain a stable temperature in the bar.
2. Precondition the bar at 50 Hz at maximum test voltage. The test time was reduced to the second frequency to ensure stable 50-Hz conditions throughout the sweep at different temperatures.
3. Increase the voltage stepwise from zero until the maximum voltage is reached.
4. Reduce the voltage stepwise until zero voltage.
5. Repeat step 2 to 4 at lower frequencies.

Table 4
TEST PARAMETERS FOR THE PD TESTING

Test parameter	RR	VPI	VPI back-up
Frequency range	0.1 Hz, 1 Hz and 50 Hz		
Maximum voltage	$1.5U_0$	$1.6U_0$	$1.2U_0$
Number of voltage steps	10	10	3*
Preconditioning, 1st time	5 min	5 min	5 min
Preconditioning, 2nd+ time	10 s	10 s	5 min
Step length	10 s or 10 T	30 s or 30 T	9000 T
Temperature	20°C to 155°C	20°C to 130°C	30°, 70°, and 130°C
Time between temperatures	2 h	1 d	1 d

*{PDIV+0.1U_0, U_0, 1.2 U_0}

IV. Results

A. Dielectric properties

The complex permittivity as a function of frequency at three different temperatures for both RR and VPI bars is presented in Fig. 3. Vertical lines indicate 0.1 Hz, 1 Hz, and 50 Hz. The shown permittivities are representative of all RR and VPI bars, respectively. The general trend in Fig. 3 is that the complex permittivity decreases with frequency and increases with temperature. The complex permittivity is similar for RR and VPI above 0.1 Hz.

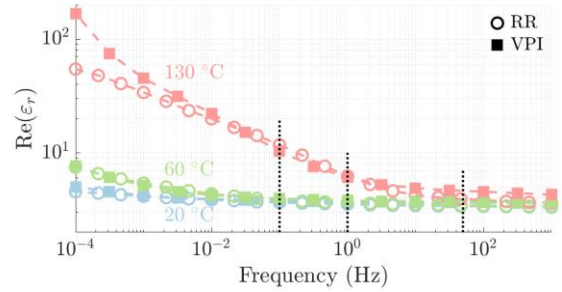

a) Real part of complex permittivity

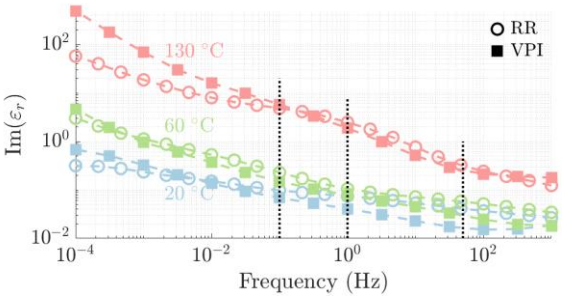

b) Imaginary part of complex permittivity

Fig. 3: Measured complex permittivity of RR and VPI bars at indicated temperatures as a function of frequency at 200 V. Vertical lines indicate 0.1 Hz, 1 Hz, and 50 Hz.

The DC conductivity of the RR bars and VPI bars were measured at room temperature to be 10^{-16} S/m and 10^{-14} S/m, respectively. The variation between the different samples was insignificant. Such low DC conductivities do not influence the extended abc-model (2); it thus can be considered purely capacitive or to includes dielectric loss at the combination of high temperatures and low frequencies.

B. Phase-resolved PD Patterns

Typical phase-resolved PD (PRPD) patterns for VPI and RR are shown in Fig. 4 at 0.1 Hz and 50 Hz and 20 °C and 130 °C. The patterns clearly indicate that we are investigating void and delamination discharges. The overall trends demonstrate that the PD activity increases with temperature for RR and decreases for VPI. The shapes of the PD patterns do not change with temperature; thus, there are mainly voids and delaminations present.

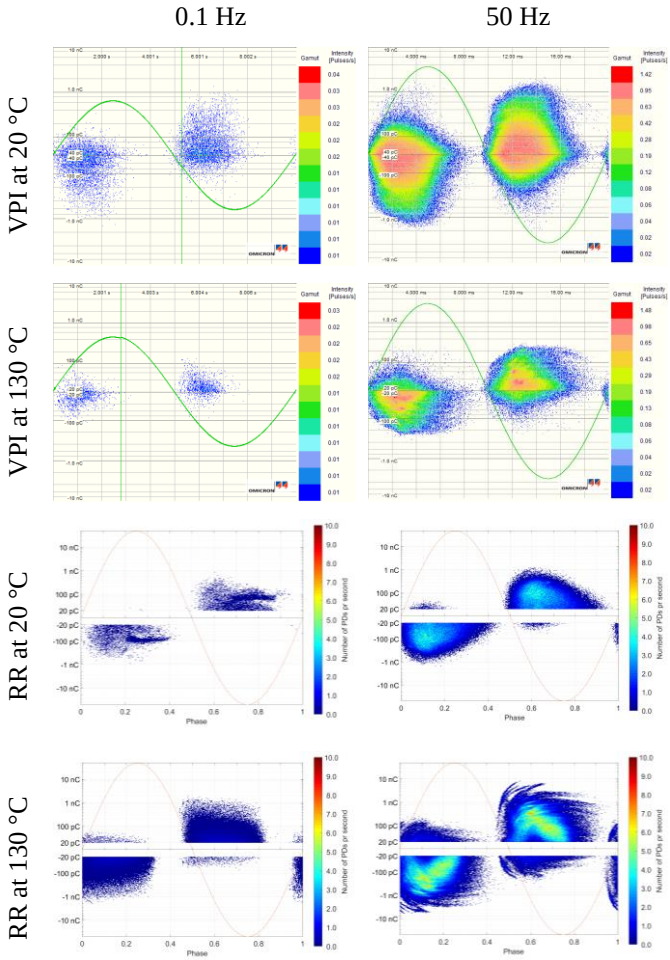

Fig. 4: Typical PRPD patterns at 0.1 Hz and 50 Hz for RR and VPI at 20 °C and 130 °C. The applied voltage is such that the average electric field is equal for VPI and RR: 4.5 kV/mm.

C. Partial Discharge Inception Voltage - PDIV

PDIV was defined as the first voltage at which a sustaining PD activity of minimum 100 pC occurred. This is a basic parameter defining if there are PDs or not in the system. The first PD inception is related to the weakest defects in the insulation system. The average measured PDIV for RR and VIP are shown in Fig. 5. For the RR bars, the PDIV at 50 Hz is almost temperature independent, whereas the PDIV at 0.1 Hz and 1 Hz decreases with temperature. For the VPI bars, the trend is the opposite, the PDIV increases with temperature at 0.1 Hz, 1 Hz, and 50 Hz. Only three

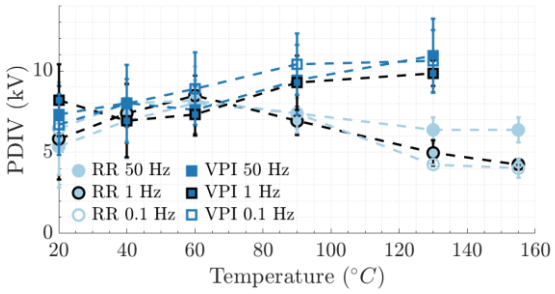

Fig. 5: Average PDIV as a function of temperature at 50 Hz for RR and VPI.

temperatures were tested for the VPI back-up bars, and they align well with the other VPI bars presented in Fig. 5.

D. The apparent charge

The apparent charge is a calibrated measure of the PD magnitude. A generator bar may contain many unknown and undefined defects, which produce PDs with a variety of magnitudes and intensities. A typical graph for PD repetition rate per period as a function of indicated voltages is given in Fig. 6. It is seen that there is a large spread in the magnitudes, with a few large and many small PDs. The amplitude in the distribution seems to increase with the same proportionality factor as a function of applied voltage. The shapes of the curves in the presented figure were qualitatively similar for all tested bars at all frequencies and temperatures. The distributions in Fig. 6 are challenging to compare directly between different temperatures, frequencies, etc. Therefore, derived quantities, like the maximum apparent charge and total apparent charge, related to available energy in the voids, can be used.

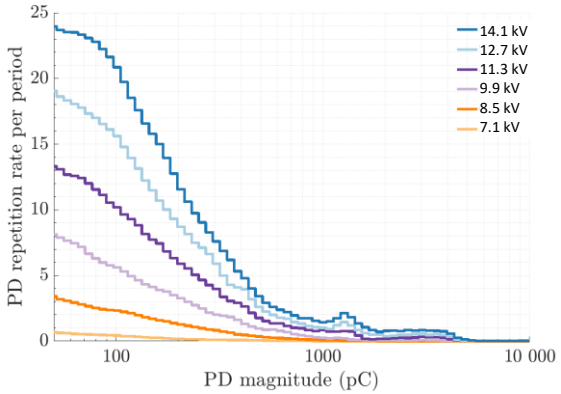

Fig. 6: A typical graph for PD repetition rate per period as a function of PD magnitude at indicated voltages. This is a representative figure for all tested samples, exemplified by a RR bar close to the HV terminal at 90 °C.

E. The maximum apparent charge

The measured maximum apparent charges are shown in Fig. 7 as a function of temperature at 0.1 Hz, 1 Hz, and 50 Hz. The applied voltage is such that the average electric field in the insulation in the two bar types is 4.5 kV/mm. For the RR samples, the maximum apparent charge increases from 1 nC at 20 °C to 5.5 nC at 130 °C at 50 Hz, while there is no significant increase at 0.1 Hz. For VPI bars, the trend is the opposite, with the maximum apparent charge decreasing with temperature. There is no significant difference at different temperatures, neither at 0.1 Hz nor at 50 Hz for the VPI bars.

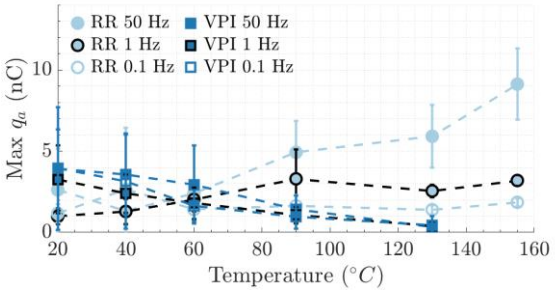

Fig. 7: Measured maximum apparent charge vs temperature at E = 4.5 kV/mm (13.6 kV_{pk} and 16.7 kV_{pk}) for the RR and VPI. measured at 0.1 Hz and 50 Hz.

F. The total apparent charge per period

The measured total apparent charge per period can be treated as a measure of the available energy in the discharged voids in the bars. The average total apparent charge per period-volume as a function of temperature at indicated frequencies for the RR and VPI bars are given in Fig. 8. The total apparent charge per period was normalized to per volume to easier compare the PD activity between the samples of different size (insulation volume). The total apparent charge per period for VPI decreases with temperature as does the maximum apparent charge for all frequencies. Conversely, for RR, the total apparent charge per period increases with temperature, as for the maximum apparent charge. There are some differences related to the applied frequency. The highest increase with temperature for the maximum apparent charge was at 50 Hz; particularly, a significant increase at 130 °C at 1 Hz in the total apparent charge per period was observed.

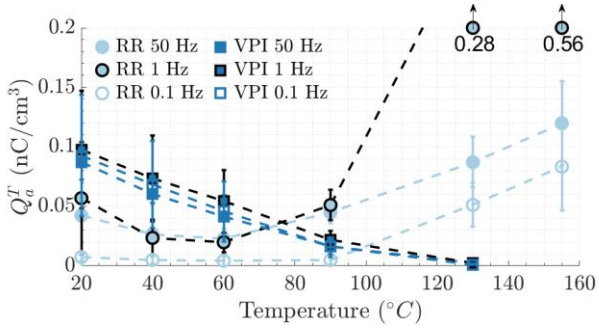

Fig. 8: General trend of the measured total apparent charge per volume insulation as a function of temperature at indicated frequency at E = 4.5 kV/mm (13.6 kV_{pk} and 16.7 kV_{pk}) for RR and VPI measured at 0.1 Hz and 50 Hz.

G. Typical cross sections with voids and delaminations

More than 100 cross-sections from the tested bars were made. From visual inspection in an optical microscope, it was found that many cross-sections did not have observable voids, while others had visible defects, which are presented in this section. In the RR bars, the observed voids were in the conductive putty in the wedges between the conductors, several millimeters in size of order. The observed voids in VPI bars were smaller and located on the corners with 0.1 mm size of order. Both RR and VPI had delaminations, whose widths in the cross-section were of several millimeters and heights were typically of 0.1-0.2 mm. Typical voids are illustrated in the micrographs in Fig. 9 for RR and in Fig. 10 for VPI.

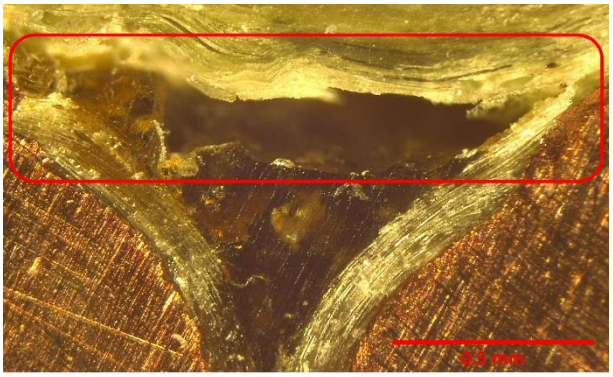

a) Most frequent void in RR: Voids in the conductive paste close to the copper conductor. Height: 0.2 mm and width = 1 mm.

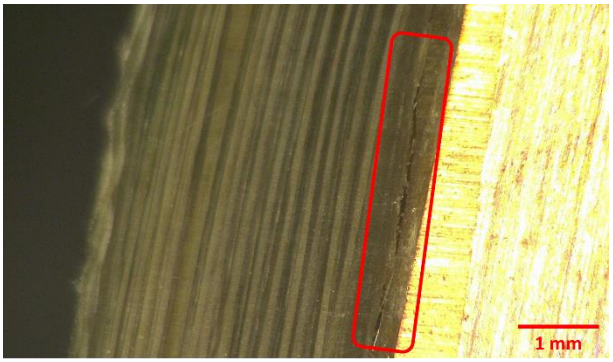

b) Delamination in the mainwall insulation. Height: 0.6 mm and width: 5 mm.

Fig. 9: Selected parts of cross sections of a RR bar.

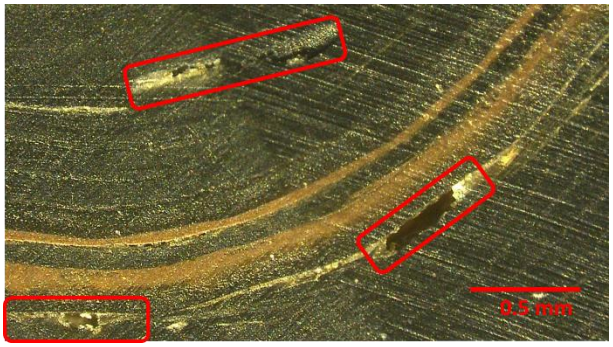

a) Small voids in VPI in the mainwall insulation. Height: 0.07 mm and width = 0.2 mm.

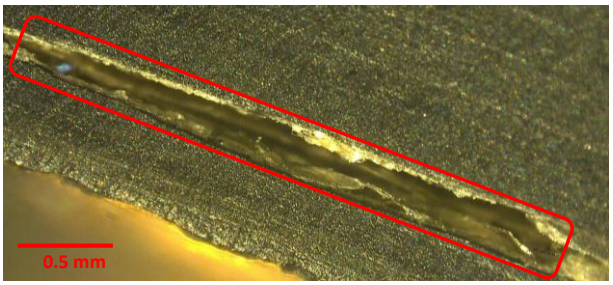

b) Delamination in the mainwall insulation. Height: 0.2 mm and width: 3 mm.

Fig. 10: Selected parts of cross sections of a VPI bar.

III. DISCUSSION

A. The PDIV

The measured PDIV is a measure of the voltage distribution for the void with the lowest breakdown voltage. Equation (2) describes a general relation between the void voltage and the applied voltage if the geometry is known. All involved material and geometry parameters are, in fact, temperature dependent. The void breakdown voltage U_s is, by the Paschen law and the ideal gas law, temperature dependent, and a higher breakdown voltage is expected at higher temperatures in enclosed voids. The measured dielectric response ε_b^* increases with temperature, as shown in Fig. 3. Similarly, it is expected that the involved conductivities increase with temperature, according to Arrhenius law. The temperature dependence of such parameter variance on PDIV is shown in Fig. 11. From this figure, it is reasonable that the reduced PDIV at higher temperatures at 0.1 Hz and 1 Hz for the RR bars is governed by the complex permittivity presented in Fig. 3 used in (2). The complex permittivity for both VPI and RR are comparable. It is, therefore, interesting to observe a totally different temperature-dependent PDIV as the RR samples follow the expected temperature dependencies based on dielectric response and (2), while the VPI does not follow the same trend.

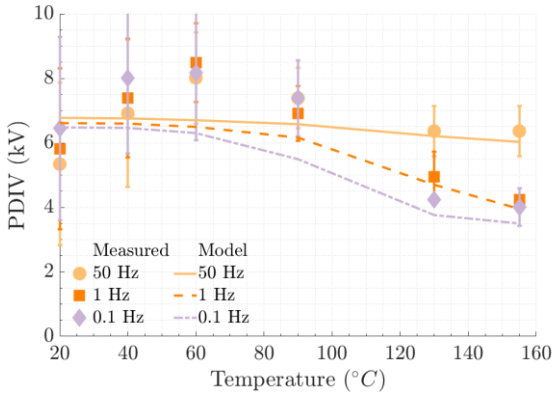

Fig. 11: PDIV according to (2) for RR with measured complex permittivity. The void gap distance is set to 0.5 mm.

Several different mechanisms may have led to the observed different trends in PDIV. First of all, the voids in RR are larger than the VPI, as seen in the micrographs in Fig. 9 and Fig. 10. The voids are located in the mainwall insulation for VPI but close to the conductors between the conductive putty and insulation for RR. Delaminations are seen in both systems in the mainwall insulation. The binder material in VPI is epoxy, whereas RR has polyester as binder material. Another possible cause can be a possible decreased void resistance for the VPI bars. The smaller voids can also be assumed enclosed, in which the pressure rise with temperature, according to ideal gas law (resulting in about 1-2 kV increase in PDIV at 155 °C). This is not sufficient to explain the increased PDIV, as a smaller void gap distance is required for sufficiently increasing the PDIV, as shown in Fig. 12. For a sufficient fit, the void gap distances must decrease by 5 % at 90 °C, 20 % at 130 °C, and 35 % at 155 °C to be able to fit measured values, which doesn't seem reasonable because a much higher thermal expansion than what

is for copper and insulation on a macroscopic level (< 1 %) is needed. It is therefore not possible to claim any single mechanism responsible for the increase in PDIV for VPI, but the correlating observed and estimated trends indicate that there is a decreasing void resistance with temperature, in accordance with Arrhenius, and a quenching of the voids as the temperature increases.

Another possibility is that some voids are quenched by a low resistance at different voltage levels. This can result in an increased PDIV as new voids with a higher PDIV act as PD sources, and thus govern PDIV for the complete insulation system. Then the main difference between the RR and VPI is that the voids in RR are not short-circuited at increasing temperature, whereas the voids in VPI are gradually short-circuited with a distribution of voids with different PDIV. The voids with the lowest PDIV seem to be short-circuited before the voids with higher PDIV.

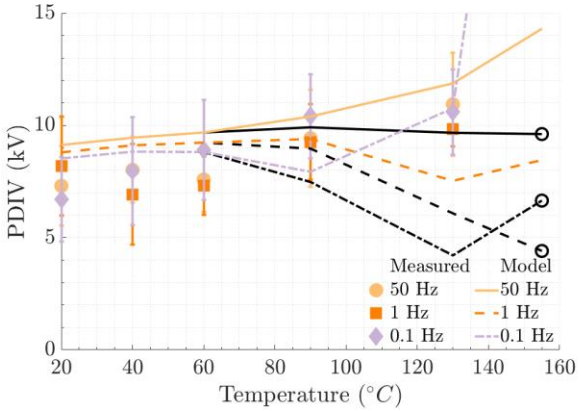

Fig. 12: PDIV according to (2) for VPI with measured complex permittivity. The void gap distance is 0.1 mm. Here, the pressure increased with temperature in line with ideal gas law. The void conductivity was here chosen to be $3 \cdot 10^{-16}$ S/m at 20 °C with an activation energy of 0.9 eV, black curves with a circle at 155 °C. The colored curves include a reduction in void gap distance of 5 % at 90 °C, 20 % at 130 °C, and 35 % at 155 °C.

B. The measured apparent charge magnitude

The cross sections in Fig. 9 and Fig. 10 illustrate that there are many small voids inside the mainwall insulation of the stator bars. The observed apparent charge magnitude distribution in Fig. 6 seems, therefore, reasonable. However, the total apparent charge is linear with voltage above the PDIV. This is not expected, as this requires that the voids inside the insulation have the same PDIV and a constant void capacitance discharge as a function of voltage. This is not in line with the extended abc-model as the maximum apparent charge as a function of voltage is strictly increasing, thus indicating larger and larger voids are activated when the voltage increases – and would require further work to prove.

The temperature dependence of the maximum apparent charge (Fig. 7) and total apparent charge per period-volume (Fig. 8) are inversely proportional to the PDIV, thus dependent on the void voltage and available electrical energy stored in the voids, as described in (7) and (8). The frequency-independent total apparent charge per period-volume for the VPI bars indicate that voids must decrease in size, either physically or by means of short-circuiting, due to sufficiently higher surface conductivity at higher temperatures. For the RR bars, the total apparent charge per period-volume is frequency independent between 1 Hz and 50 Hz below 90 °C. The apparent charge magnitude at 0.1 Hz is much lower than at higher frequencies. The low apparent charge magnitude at 0.1 Hz might originate from a relatively low void resistance that partly short-circuit the voids but is not sufficient to completely avoid ignition in some voids. The high increase in apparent charge magnitude at 1 Hz can be explained by the strong increase in dielectric losses, in which a larger portion of the applied voltage is across the void.

The significant increase can be related to the increase in complex permittivity; thus, a higher fraction of the applied voltage is across the void. This enables more PDs to occur within the same period. If this was the case, then the total apparent charge at 0.1 Hz would be very high, which is not the case. This might be explained by using (2) for the idealized void by a decreased non-measurable void resistance at higher temperatures that, to a larger extent, quenches the void voltage, which is then more influential at 0.1 Hz than at 1 Hz.

C. Implications for condition assessment

The objective of this work is to investigate if off-line VLF PD measurements are applicable as a condition assessment method probing PD-activity for hydro generators since this will make PD measurements easier to perform and more cost-effective. The measured PD activity at VLF must be representative and/or translatable to PD activity during service for accurate assessment. It is here found that PD-parameters relevant for condition assessment varies with voltage-frequency and temperature. Further, the temperature dependencies are also opposite for the two insulation systems tested, i.e., RR and VPI.

PDIV:

- For VPI, PDIV increases with temperature – as expected. There is little difference between 0.1, 1, and 50 Hz – and VLF is thus representative at all temperatures.
- For RR, PDIV decreases with temperature. For temperatures above 90 °C, the decrease is significantly larger for 0.1 and 1 Hz compared to 50 Hz. VLF is representative below 90 °C.

Apparent charge and derived quantities

- For VPI, the maximum and total apparent charge per period decrease with temperature, and there is no significant frequency dependency. VLF is representative.
- For RR, there is a slight increase in maximum and total apparent charge per period with temperature. VLF is representative of the maximum apparent charge up to 60 °C but not the total apparent charge per period-volume, which has a much lower value at VLF.

Global dielectric properties, such as complex permittivity (tan δ) and DC conductivity, are similar for RR and VPI. It is, therefore, not likely that global dielectric properties can explain the differences in the PD activity for RR and VPI insulation systems.

From a study of load-cycling of RR and VPI bars from the seventies, it was found that RR bars had more delaminations

than VPI bars [22]. A difference in void size/shape and how temperature affects these dimensions as a function of temperature can thus be an explanation for the opposite temperature dependencies seen between RR and VPI insulation systems.

VLF can be used for these VPI bars, but care must be taken for RR bars according to the results in this work. More work is needed on RR insulation systems as many generators from the 60 and 70'ies have RR insulation systems – e.g., by doing load cycling studies to investigate the dynamics of temperature change.

III. Conclusions

The tests revealed that the RR and VPI bars have opposite frequency dependency of PD-behavior in some cases. While PDIV of RR bars at 0.1 Hz decrease with temperature and at 50 Hz is temperature independent, PDIV for all frequencies for VPI increase with temperature. For the maximum and total apparent charge per period, the opposite temperature dependency was seen. The implication of this is at a direct comparison of PD parameters at VLF and PLF cannot be done for all machines without considering temperature when measurements are performed on insulation systems. If a new regime of condition assessment is implemented by applying VLF PD measurements, trending of relevant parameters could be undertaken as for conventional PLF PD measurements. The strength of condition assessment by VLF PD measurements is compact measurement setup and affordability, which should make it possible to extend the use of PD measurements as a low-cost alternative on hydro generators and other rotating machines. An improved condition assessment can also be performed at an extended frequency range and at different temperatures to extract more information from PD measurements. Also, further research on characterizing voltage-frequency dependency on other common defects in stator bars is needed.

Acknowledgment

Hydro Energi AS is acknowledged for providing generator bars available for research in this work.

References

[1] "IEC TS 60034-27:2006, Off-line partial discharge measurements on the stator winding insulation of rotating electrical machines," 2006.

[2] "IEEE Std 1434-2014 (Revision of IEEE Std 1434-2000), IEEE Guide for the Measurement of Partial Discharges in AC Electric Machinery," 2014. doi: 10.1109/IEEESTD.2014.6973042.

[3] "IEEE Std 433-2009 (Revision of IEEE Std 433-1974), IEEE Recommended Practice for Insulation Testing of AC Electric Machinery with High Voltage at Very Low Frequency," 2009. doi: 10.1109/IEEESTD.2009.5423694.

[4] N. Taylor, "Measured and modeled capacitance, loss and harmonics in stator insulation with nonlinear stress control," *IEEE Transactions on Dielectrics and Electrical Insulation*, vol. 22, no. 6, pp. 3133–3145, 2015, doi: 10.1109/TDEI.2015.005260.

[5] G. C. Stone, E. A. Boulter, I. Culbert, and H. Dhirani, *Electrical Insulation for RotatingMachines Design, Evaluation, Aging, Testing, and Repair*, 1st ed. New York: Wiley Interscience, 2004.

[6] T. Aakre and E. Ildstad, "AC Breakdown Voltage of 50-Year-Old Service Aged Hydro Power Generator Stator Bars," *NORD-IS*, vol. 27, no. 1, Jul. 2022, doi: 10.5324/nordis.v27i1.4714.

[7] E. Kantar, E. Eberg, and S. Hvidsten, "Effects of Frequency and Temperature on Partial Discharge Characterization of Stator Windings," in *2020 IEEE Conference on Electrical Insulation and Dielectric Phenomena (CEIDP)*, East Rutherford, NJ, USA, Oct. 2020, pp. 369–373. doi: 10.1109/CEIDP49254.2020.9437438.

[8] E. Eberg, T. G. Aakre, G. Berg, and S. Hvidsten, "Comparison of Offline VLF PD Measurements and Online PD Measurements on a 50-Year-Old Hydrogenerator Stator in Norway," in *2018 IEEE Electrical Insulation Conference (EIC)*, San Antonio, TX, Jun. 2018, pp. 542–546. doi: 10.1109/EIC.2018.8481080.

[9] R. Vogelsang, T. Weiers, K. Frohlich, and R. Brutsh, "Electrical breakdown in high-voltage winding insulations of different manufacturing qualities," *IEEE Electr. Insul. Mag.*, vol. 22, no. 3, pp. 5–12, May 2006, doi: 10.1109/MEI.2006.1639024.

[10] R. P. Nair, B. V. Sumangala, B. Nageshwar Rao, and Thirumurthy, "Effect of temperature on slot discharge pattern measured in stator coils at variable frequency sinusoidal voltage excitation," presented at the Proceedings of the IEEE International Conference on Properties and Applications of Dielectric Materials, 2018, vol. 2018-May, pp. 257–261. doi: 10.1109/ICPADM.2018.8401259.

[11] R. P. Nair and S. B. Vishwanath, "Analysis of partial discharge sources in stator insulation system using variable excitation frequency," *IET Science, Measurement and Technology*, vol. 13, no. 6, pp. 922–930, 2019, doi: 10.1049/iet-smt.2018.5666.

[12] T. G. Aakre, E. Ildstad, and S. Hvidsten, "Partial Discharge Inception Voltage of Voids Enclosed in Epoxy/Mica versus Voltage Frequency and Temperature," *IEEE Transactions on Dielectrics and Electrical Insulation*, vol. 27, no. 1, pp. 190–197, 2020, doi: 10.1109/TDEI.2019.008394.

[13] C. Forssen and H. Edin, "Partial discharges in a cavity at variable applied frequency part 1: measurements," *IEEE Trans. Dielect. Electr. Insul.*, vol. 15, no. 6, pp. 1601–1609, Dec. 2008, doi: 10.1109/TDEI.2008.4712663.

[14] C. Forssen and H. Edin, "Partial discharges in a cavity at variable applied frequency part 2: measurements and modeling," *IEEE Trans. Dielect. Electr. Insul.*, vol. 15, no. 6, pp. 1610–1616, Dec. 2008, doi: 10.1109/TDEI.2008.4712664.

[15] A. Cavallini and G. C. Montanari, "Effect of supply voltage frequency on testing of insulation system," *IEEE Trans. Dielect. Electr. Insul.*, vol. 13, no. 1, pp. 111–121, Feb. 2006, doi: 10.1109/TDEI.2006.1593409.

[16] H. Illias, G. Chen, and P. L. Lewin, "Partial discharge behavior within a spherical cavity in a solid dielectric material as a function of frequency and amplitude of the applied voltage," *IEEE Trans. Dielect. Electr. Insul.*, vol. 18, no. 2, pp. 432–443, Apr. 2011, doi: 10.1109/TDEI.2011.5739447.

[17] E. Kuffel, W. Zaengl, and J. Kuffel, *High Voltage Engineering Fundamentals, 2nd Edition*. 2000.

[18] E. J. Flynn, C. E. Kilbourne, and C. D. Richardson, "An Advanced Concept for Turbine-Generator Stator-Winding Insulation," *Trans. AIEE, Part III: Power Appar. Syst.*, vol. 77, no. 3, pp. 358–365, Apr. 1958, doi: 10.1109/AIEEPAS.1958.4499937.

[19] R. H. Schuler, "Experience with Micadur® synthetic-resin insulation for stator windings of high voltage rotating machines," in *1967 Seventh Electrical Insulation Conference*, Chicago, IL, USA, Oct. 1967, pp. 61–64. doi: 10.1109/EIC.1967.7468758.

[20] G. Berg, E. Eberg, and S. Hvidsten, "Partial Discharge Characterisation of Stator Windings Taken from a 50-year-old Norwegian Hydrogenerator," in *2019 IEEE Electrical Insulation Conference (EIC)*, Calgary, AB, Canada, Jun. 2019, pp. 168–171. doi: 10.1109/EIC43217.2019.9046527.

[21] T. A. Ve, F. Mauseth, and E. Ildstad, "Effect of water content on the conductivity of XLPE insulation," in *2012 Annual Report Conference on Electrical Insulation and Dielectric Phenomena*, Montreal, QC, Oct. 2012, pp. 649–653. doi: 10.1109/CEIDP.2012.6378864.

[22] M. Istad, M. Runde, and A. Nysveen, "A Review of Results From Thermal Cycling Tests of Hydrogenerator Stator Windings," *IEEE Trans. Energy Convers.*, vol. 26, no. 3, pp. 890–903, Sep. 2011, doi: 10.1109/TEC.2011.2127479.